Research Square

Preprints are preliminary reports that have not undergone peer review.
They should not be considered conclusive, used to inform clinical practice,
or referenced by the media as validated information.

Sphere-based representation of image-resolved porous media

Felix Buchele

felix.buchele@fau.de

Friedrich-Alexander-Universität Erlangen-Nürnberg

Thorsten Pöschel

Friedrich-Alexander-Universität Erlangen-Nürnberg

Research Article

Keywords: pore reconstruction, multi-sphere representation, porous media, pore-scale modeling, image-based reconstruction

Posted Date: September 8th, 2026

DOI: https://doi.org/10.21203/rs.3.rs-10829095/v1

License: This work is licensed under a Creative Commons Attribution 4.0 International License.
Read Full License

Additional Declarations: No competing interests reported.

Sphere-based representation of image-resolved porous media

Felix Buchele[1*] and Thorsten Pöschel[1]

[1*]Institute for Multiscale Simulation, Friedrich-Alexander-Universität Erlangen-Nürnberg, Cauerstraße 3, Erlangen, 91058, Germany.

*Corresponding author(s). E-mail(s): felix.buchele@fau.de;
Contributing authors: thorsten.poeschel@fau.de;

Abstract

The Multi-Sphere Shape (MSS) algorithm is applied to generate sphere-based representations of porous media directly from segmented volumetric image data. The solid or void phase is approximated by overlapping spheres, providing a simplified representation for particle-based simulations. The sphere centers lie on the medial axis of the selected phase without requiring explicit medial-axis extraction. The approach is demonstrated for the pore space of a ceramic foam reconstructed from computed tomography (CT) data, where 22,468 spheres represent 95% of a volume comprising 64 million voxels. For sphere-dominated morphologies, the sphere sizes, overlaps, and connectivity additionally provide structural descriptors such as pore sizes, throat areas, and coordination numbers. The resulting representation therefore combines a simplified simulation model with direct access to structural information.

Keywords: pore reconstruction, multi-sphere representation, porous media, pore-scale modeling, image-based reconstruction

Article Highlights.

- Porous structures from 3D image data can be represented by overlapping spheres.
- The representation retains spatial structure while providing direct information on size and connectivity.
- The sphere model can be used in particle-based simulations.

1 Introduction

Simulations of transport, heat transfer, and chemical reactions in porous media require a suitable representation of the underlying structure. Such representations can be obtained directly from three-dimensional image data, such as micro-computed tomography (micro-CT) or focused ion beam–scanning electron microscopy (FIB-SEM), and have been used for pore-scale simulations of diffusion and reaction (Karakaya et al. 2016; Ranut et al. 2014; Raeini et al. 2014; Maes and Menke 2022). However, voxel data and meshes derived from them can be computationally demanding for direct use in simulations (Bultreys et al. 2016; Blunt et al. 2013). In addition to direct simulation, volumetric image data provide access to structural information through geometrical, topological, and network-based characterization methods (Armstrong et al. 2019).

Pore-network models provide a common simplification of image-resolved pore structures by representing the void space as pore bodies connected by throats (Gostick et al. 2016). Such networks can be extracted from segmented image data using watershed methods (Gostick 2017; Gostick et al. 2019), maximal-ball methods based on maximal inscribed spheres (Silin and Patzek 2006; Dong and Blunt 2009; Arand and Hesser 2017), or medial-axis methods based on a skeleton of the pore space (Lindquist et al. 1996; Al-Raoush and Willson 2005; Jiang et al. 2007). Approaches combining medial-axis and maximal-ball concepts have also been developed (Yi et al. 2017). In maximal-ball methods, the spheres are used to identify pores and throats and thereby construct a pore network (Dong and Blunt 2009; Yi et al. 2017). The resulting networks provide compact descriptions of pore sizes and connectivity, but reduce the spatial pore structure to discrete pore and throat elements.

Sphere- and inverse-sphere-based models provide an alternative simplification in which the solid or void phase is represented explicitly by a set of spheres. Such representations have been used for particle packings in catalyst pellets (Rao and Coppens 2012; Reyes and Iglesia 1991) and washcoats (Pereira et al. 2014; Kočí et al. 2010), packed beds (Shi et al. 2019; Calis et al. 2001), and open-cell foams (Smorygo et al. 2011; Mühlbauer et al. 2026). In particular, inverse sphere packings have been used to represent open-cell foam structures (Smorygo et al. 2011) and as boundary descriptions for particle-based simulations of flow and catalytic reactions (Mühlbauer et al. 2026). Depending on the structure of interest, either the solid phase can be represented by spheres or the void phase by an inverse sphere packing.

The Multi-Sphere Shape (MSS) algorithm generates sphere-based representations by approximating a target volume with a finite set of overlapping spheres. Originally developed to generate multi-sphere particle models for Discrete Element Method (DEM) simulations, MSS can approximate complex target volumes with comparatively few spheres (Buchele et al. 2026a). The sphere centers generated by MSS lie on the medial axis and therefore correspond to centers of maximal inscribed spheres, without requiring explicit extraction of the medial axis (Moradian et al. 2026a). Open-source implementations of MSS are available in Python (Buchele et al. 2026b) and C++ (Moradian et al. 2026b). In previous work, inverse sphere representations generated with MSS were used to extract pore-size, overlap, and connectivity information for the generation of parameterized porous model structures (Buchele et al. 2024).

Here, we apply MSS directly to segmented volumetric images of porous media to obtain sphere-based representations of either the solid or void phase. In contrast to pore-network extraction, the overlapping spheres themselves form the spatial representation rather than serving only to identify discrete pores and throats. The resulting representation can be used directly in suitable particle-based simulations, while sphere sizes, overlaps, and adjacency additionally provide structural information. We demonstrate the approach for the pore space of a ceramic foam reconstructed from CT data and quantify the resulting representation and structural descriptors.

2 Sphere-based representation of porous media

Starting from segmented volumetric image data, MSS can be applied to either the solid or the void phase of a porous medium, as illustrated in Figure 1. Application to the solid phase yields a sphere-based representation of the solid structure, whereas application to the void phase yields an inverse sphere representation of the pore space. In both cases, the selected phase defines a binary target volume V that is approximated by the union of N spheres,

$$V_{\mathrm{MSS}} = \bigcup_{i=1}^{N} B\left(\vec{x}_i, r_i\right) , \tag{1}$$

where $\vec{x}_i$ and r_i denote the center and radius of sphere i, respectively.

For the binary target volume, MSS computes the Euclidean distance transform (EDT). Local maxima of the EDT define maximally inscribed spheres and provide an initial representation of the target volume. The remaining mismatch between the target volume and the sphere-based representation is then evaluated, and additional spheres are placed iteratively to reduce this mismatch. The procedure continues until a prescribed mismatch or minimum sphere radius is reached. A detailed description of the MSS algorithm is given by Buchele et al. (2026a).

The centers of the spheres generated by MSS lie on the medial axis of the target volume (Moradian et al. 2026a). This connects the representation to maximal-ball methods used for pore-network extraction (Silin and Patzek 2006; Dong and Blunt 2009; Arand and Hesser 2017; Yi et al. 2017). In these methods, maximal balls are used to identify pores and throats and construct a pore network (Dong and Blunt 2009; Yi et al. 2017). In MSS, by contrast, the union of the spheres itself approximates the target volume. The spatial extent of the represented phase is therefore retained, while connectivity information can be obtained directly from sphere overlaps.

Two spheres i and j are connected if they overlap,

$$|\vec{x}_i - \vec{x}_j| < r_i + r_j \, . \tag{2}$$

The sphere representation therefore also defines an adjacency graph, with spheres as vertices and overlaps as edges. Sphere radii provide local length scales of the represented volume, while pairwise overlaps characterize the connections between neighboring spheres. For sphere-dominated pore structures, these quantities can be interpreted as pore sizes, throat areas, and pore connectivity. For more general structures, an individual sphere need not correspond to a distinct physical pore. In this case, the

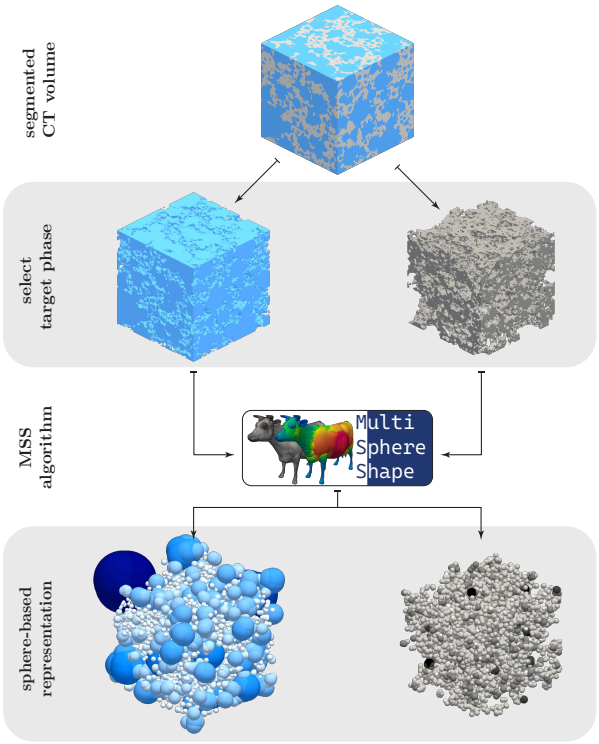


Fig. 1 Sphere-based representation of porous media using MSS. Starting from segmented volumetric image data, either the solid or the void phase is selected as the target volume. Application of MSS to the solid phase yields a sphere-based representation of the solid structure, whereas application to the void phase yields an inverse sphere representation of the pore space.

sphere set remains a simplified spatial representation of the solid or void phase, but the properties of individual spheres and overlaps should not generally be identified with physical pore and throat properties.

3 Application to a ceramic foam

3.1 Image data and sphere-based representation

The sphere-based representation is demonstrated for a foamed ceramic. Figure 2 shows a microscopy image of the material, a slice of the tomographic image, and the corresponding segmented solid and void phases. The segmented CT data serve as input to MSS. Here, MSS is applied to the void phase, resulting in an inverse sphere representation of the pore space.

The analyzed volume has dimensions of 3.14 mm × 3.14 mm × 3.14 mm at a voxel size of 7.85 µm, corresponding to $400^3 = 64$ million voxels. The minimum sphere radius was set to $r_{\min} = 23.55\,\mu\text{m}$, corresponding to 3 voxels. The resulting sphere-based representation consists of 22 468 spheres.

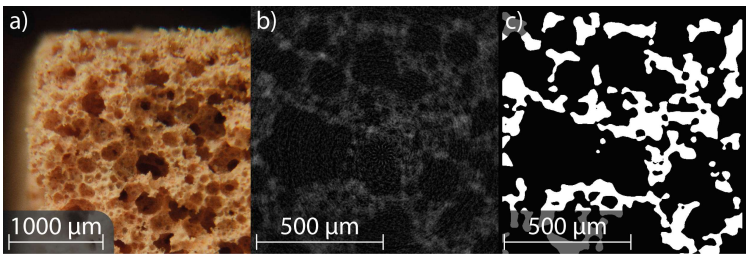


Fig. 2 Input data for the sphere-based representation of the foamed ceramic: a) microscopy image of the material, b) slice of the tomographic image, and c) segmented solid and void phases

Figure 3 compares the segmented pore space with its sphere-based representation and shows their mismatch. The representation reproduces the overall pore structure, including the principal connections visible in the segmented volume. Deviations occur primarily at irregular pore boundaries and at narrow constrictions that cannot be represented by spheres above the prescribed minimum radius.

The fraction of the segmented pore space covered by the sphere-based representation is defined as

$$C = \frac{|V \cap V_{\mathrm{MSS}}|}{|V|}, \tag{3}$$

where $|\cdot|$ denotes volume. For the present reconstruction, $C = 0.95$, i.e., 95% of the segmented pore volume is contained in the sphere-based representation.

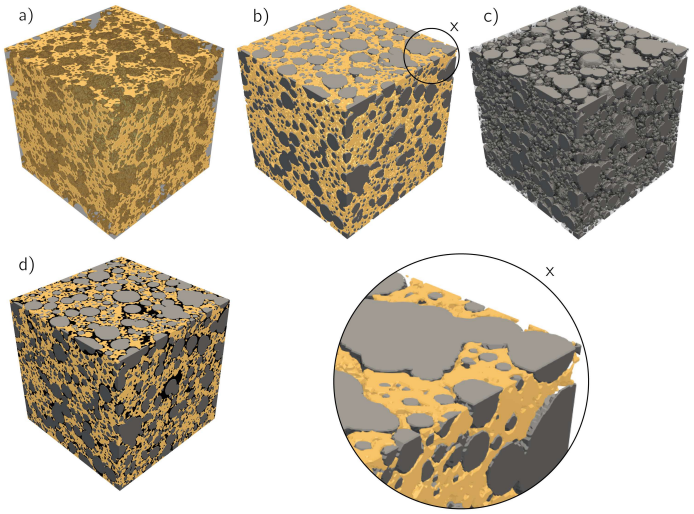


Fig. 3 Comparison of the segmented pore space and its sphere-based representation: a) segmented solid matrix, b) overlay of the solid matrix and the sphere-based representation of the pore space, c) sphere-based representation of the pore space, d) mismatch between the segmented and represented pore space, and x) magnified detail of the mismatch

3.2 Structural descriptors

In addition to providing a spatial representation of the pore volume, the overlapping spheres contain information about the local size and connectivity of the represented structure. Figure 4 shows the sphere-based representation of the ceramic foam, with the spheres colored according to the size of the connected component to which they belong.

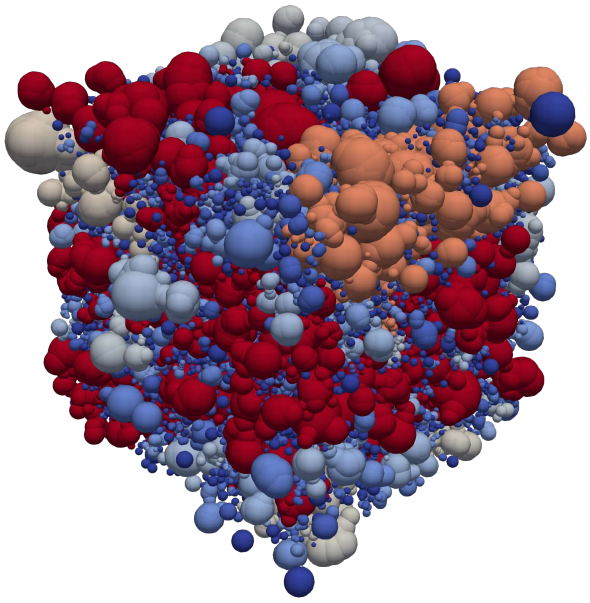


Fig. 4 Sphere-based representation of the pore space of the foamed ceramic. The spheres are colored according to the size of the connected component to which they belong.

For the sphere-dominated pore structure considered here, individual spheres provide a measure of the local pore size. We therefore define the pore diameter associated with sphere i as

$$d_i = 2r_i \,. \tag{4}$$

For two overlapping spheres, the area of their intersection provides a corresponding measure of the connection between neighboring pores. With

$$d_{ij} = |\vec{x}_i - \vec{x}_j| \,, \tag{5}$$

the radius r_{ij} of the intersection circle is given by

$$r_{ij}^2 = r_i^2 - \left(\frac{d_{ij}^2 + r_i^2 - r_j^2}{2d_{ij}} \right)^2 \,, \tag{6}$$

and the corresponding throat area is

$$A_{ij} = \pi r_{ij}^2 \,. \tag{7}$$

The resulting pore-diameter and throat-area distributions are shown in Figure 5.

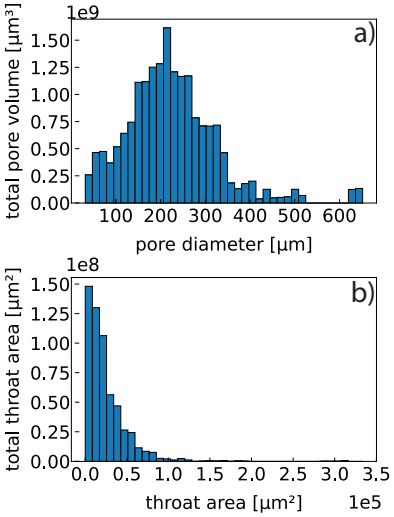


Fig. 5 Local structural descriptors obtained from the sphere-based representation: a) pore-diameter distribution and b) throat-area distribution

Connectivity follows directly from the adjacency graph defined by the sphere overlaps according to Equation (2). The coordination number k_i of sphere i is the number of spheres overlapping sphere i. Connected components are obtained from the same adjacency graph and identify mutually connected regions of the sphere representation. Figure 6 shows the distributions of connected-component sizes and coordination numbers for the reconstructed pore space.

The interpretation of these quantities as pore diameters, throat areas, and pore coordination numbers relies on the sphere-dominated structure of the present material. For more general pore structures, sphere radii, overlaps, and adjacency remain well-defined properties of the sphere representation, but need not correspond directly to individual physical pores and throats.

The structural descriptors obtained from the sphere-based representation can also serve as input for the generation of parameterized porous model structures. In previous work (Buchele et al. 2024), pore-size, throat-area, and connectivity information obtained from inverse sphere representations was used to generate model structures with prescribed structural properties. Figure 7 shows examples generated with different porosities. This provides a route from image-resolved porous structures through their sphere-based representation and structural descriptors to parameterized model structures. The resulting structures and their transport properties were validated against experimental measurements by Buchele et al. (2024).

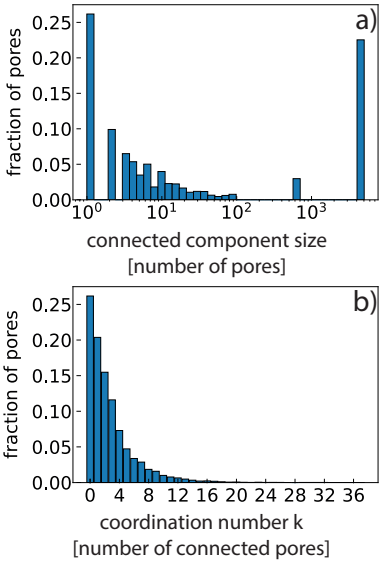


Fig. 6 Connectivity descriptors obtained from the sphere-based representation: a) connected-component size distribution and b) coordination-number distribution.



Fig. 7 Parameterized porous model structures generated from structural descriptors obtained from the sphere-based representation, shown for different porosities. The model-generation procedure and its validation are described by Buchele et al. (2024)

4 Conclusions

The Multi-Sphere Shape algorithm MSS (Buchele et al. 2026a,b; Moradian et al. 2026a,b) provides a direct route from segmented volumetric images of porous media to sphere-based representations of the solid or void phase. In contrast to a reduction to discrete pore and throat elements, the overlapping spheres retain a spatial representation of the selected phase while simultaneously defining an adjacency graph through their overlaps.

For the ceramic foam considered here, the pore space of a CT volume comprising 64 million voxels was represented by 22 468 spheres, covering 95% of the segmented pore volume. For sphere-dominated structures, the sphere radii, overlaps, and adjacency can additionally be interpreted in terms of pore sizes, throat areas, and pore connectivity. The same descriptors can serve as input for the generation of parameterized porous model structures.

The sphere-based representation thus provides a reduced spatial model derived directly from volumetric image data. It can be used as a boundary representation in suitable particle-based simulations while retaining access to structural information through the properties and connectivity of the constituent spheres.

References

Al-Raoush R, Willson C (2005) Extraction of physically realistic pore network properties from three-dimensional synchrotron x-ray microtomography images of unconsolidated porous media systems. Journal of Hydrology 300(1):44–64. https://doi.org/10.1016/j.jhydrol.2004.05.005

Arand F, Hesser J (2017) Accurate and efficient maximal ball algorithm for pore network extraction. Computers & Geosciences 101:28–37. https://doi.org/10.1016/j.cageo.2017.01.004

Armstrong RT, McClure JE, Robins V, et al (2019) Porous media characterization using Minkowski functionals: Theories, applications and future directions. Transport in Porous Media 130:305–335. https://doi.org/10.1007/s11242-018-1201-4

Blunt MJ, Bijeljic B, Dong H, et al (2013) Pore-scale imaging and modelling. Advances in Water Resources 51:197–216. https://doi.org/10.1016/j.advwatres.2012.03.003

Buchele F, Blank M, Pöschel T, et al (2024) Model geometries of random porous materials. International Journal of Heat and Mass Transfer 234:126074. https://doi.org/10.1016/j.ijheatmasstransfer.2024.126074

Buchele F, Pöschel T, Müller P (2026a) Multi-sphere shape generator for DEM simulations of complex-shaped particles. Powder Technology 480:122635. https://doi.org/10.1016/j.powtec.2026.122635

Buchele F, Müller P, Moradian A, et al (2026b) multisphere: A Python implementation of the multi sphere shape generator (MSS) for DEM simulations. SoftwareX 35:102836. https://doi.org/10.1016/j.softx.2026.102836

Bultreys T, De Boever W, Cnudde V (2016) Imaging and image-based fluid transport modeling at the pore scale in geological materials: A practical introduction to the current state-of-the-art. Earth-Science Reviews 155:93–128. https://doi.org/10.1016/j.earscirev.2016.02.001

Calis H, Nijenhuis J, Paikert B, et al (2001) CFD modelling and experimental validation of pressure drop and flow profile in a novel structured catalytic reactor packing. Chemical Engineering Science 56(4):1713–1720. https://doi.org/10.1016/S0009-2509(00)00400-0, 16th International Conference on Chemical Reactor Engineering

Dong H, Blunt MJ (2009) Pore-network extraction from micro-computerized-tomography images. Physical Review E 80:036307. https://doi.org/10.1103/PhysRevE.80.036307

Gostick J, Aghighi M, Hinebaugh J, et al (2016) OpenPNM: A pore network modeling package. Computing in Science & Engineering 18(4):60–74. https://doi.org/10.1109/MCSE.2016.49

Gostick JT (2017) Versatile and efficient pore network extraction method using marker-based watershed segmentation. Phys Rev E 96:023307. https://doi.org/10.1103/PhysRevE.96.023307

Gostick JT, Khan ZA, Tranter TG, et al (2019) PoreSpy: A python toolkit for quantitative analysis of porous media images. Journal of Open Source Software 4(37):1296. https://doi.org/10.21105/joss.01296

Jiang Z, Wu K, Couples G, et al (2007) Efficient extraction of networks from three-dimensional porous media. Water Resources Research 43(12). https://doi.org/10.1029/2006WR005780

Karakaya C, Weddle PJ, Blasi JM, et al (2016) Modeling reaction–diffusion processes within catalyst washcoats: I. microscale processes based on three-dimensional reconstructions. Chemical Engineering Science 145:299–307. https://doi.org/10.1016/j.ces.2016.02.004

Kočí P, Novák V, Štěpánek F, et al (2010) Multi-scale modelling of reaction and transport in porous catalysts. Chemical Engineering Science 65(1):412–419. https://doi.org/10.1016/j.ces.2009.06.068

Lindquist WB, Lee SM, Coker DA, et al (1996) Medial axis analysis of void structure in three-dimensional tomographic images of porous media. Journal of Geophysical Research: Solid Earth 101:8297–8310. https://doi.org/10.1029/95JB03039

Maes J, Menke HP (2022) GeoChemFoam: Direct modelling of flow and heat transfer in micro-CT images of porous media. Heat and Mass Transfer 58(11):1937–1947. https://doi.org/10.1007/s00231-022-03221-2

Moradian A, Buchele F, Pöschel T (2026a) Why the multi-sphere shape generator works: Medial-axis placement of spheres. arxivorg/260815457 https://doi.org/10.48550/arXiv.2608.15457

Moradian A, Buchele F, Müller P, et al (2026b) GEMSS: A C++ library for runtime multi-sphere modeling of granular particles in dem simulations. arxivorg/260815463 https://doi.org/10.48550/arXiv.2608.15463

Mühlbauer S, Strobl S, Coleman M, et al (2026) Simulation of catalytic reactions in open-cell foam structures. Chemical Engineering Science 327:123489. https://doi.org/10.1016/j.ces.2026.123489

Pereira J, Navalho J, Amador A, et al (2014) Multi-scale modeling of diffusion and reaction–diffusion phenomena in catalytic porous layers: Comparison with the 1D approach. Chemical Engineering Science 117:364–375. https://doi.org/10.1016/j.ces.2014.06.028

Raeini AQ, Blunt MJ, Bijeljic B (2014) Direct simulations of two-phase flow on micro-CT images of porous media and upscaling of pore-scale forces. Advances in Water Resources 74:116–126. https://doi.org/10.1016/j.advwatres.2014.08.012

Ranut P, Nobile E, Mancini L (2014) High resolution microtomography-based CFD simulation of flow and heat transfer in aluminum metal foams. Applied Thermal Engineering 69(1):230–240. https://doi.org/10.1016/j.applthermaleng.2013.11.056

Rao SM, Coppens MO (2012) Increasing robustness against deactivation of nanoporous catalysts by introducing an optimized hierarchical pore network—application to hydrodemetalation. Chemical Engineering Science 83:66–76. https://doi.org/10.1016/j.ces.2011.11.044, mathematics in Chemical Kinetics and Engineering International Workshop 2011

Reyes SC, Iglesia E (1991) Effective diffusivities in catalyst pellets: new model porous structures and transport simulation techniques. Journal of Catalysis 129(2):457–472. https://doi.org/10.1016/0021-9517(91)90049-A

Shi Y, Ye G, Yang C, et al (2019) Pore engineering of hierarchically structured hydrodemetallization catalyst pellets in a fixed bed reactor. Chemical Engineering Science 202:336–346. https://doi.org/10.1016/j.ces.2019.03.049

Silin D, Patzek T (2006) Pore space morphology analysis using maximal inscribed spheres. Physica A: Statistical Mechanics and its Applications 371(2):336–360. https://doi.org/10.1016/j.physa.2006.04.048

Smorygo O, Mikutski V, Marukovich A, et al (2011) An inverted spherical model of an open-cell foam structure. Acta Materialia 59(7):2669–2678. https://doi.org/10.1016/j.actamat.2011.01.005

Yi Z, Lin M, Jiang W, et al (2017) Pore network extraction from pore space images of various porous media systems. Water Resources Research 53:3424–3445. https://doi.org/10.1002/2016WR019272

Statements and Declarations

Funding

The authors declare that no funds, grants, or other support were received during the preparation of this manuscript.

Competing Interests

The authors have no relevant financial or non-financial interests to disclose.

Data Availability

The volumetric image data analyzed in this study are publicly available at https://github.com/FelixBuchele/multisphere.

Code Availability

The Python implementation of the MSS algorithm, `multisphere`, is publicly available at https://github.com/FelixBuchele/multisphere. The C++ implementation, GEMSS, is publicly available at https://github.com/aqa-arash/GEMSS.